B-spline Algebraic Diagrammatic Construction: Application to Photoionization Cross-Sections and High-order Harmonic Generation

M. Ruberti and V. Averbukh

Department of Physics, Imperial College London,

Prince Consort Road, London SW7 2AZ, United Kingdom

P. Decleva

Dipartimento di Scienze Chimiche, Universita' di Trieste,

Via Giorgieri 1, I-34127 Trieste, Italy

Abstract

We present the first implementation of the *ab initio* many-body Green's function method, algebraic diagrammatic construction (ADC), in the B-spline single-electron basis. B-spline versions of the first order [ADC(1)] and second order [ADC(2)] schemes for the polarization propagator are developed and applied to the *ab initio* calculation of static (photoionization cross-sections) and dynamic (high-order harmonic generation spectra) quantities. We show that the cross-section features that pose a challenge for the Gaussian basis calculations, such as Cooper minima and high-energy tails, are found to be reproduced by the B-spline ADC in a very good agreement with the experiment. We also present the first dynamic B-spline ADC results, showing that the effect of the Cooper minimum on the high-order harmonic generation spectrum of Ar is correctly predicted by the time-dependent ADC calculation in the B-spline basis. The present development paves the way for the application of the B-spline ADC to both energy- and time-resolved theoretical studies of many-electron phenomena in atoms, molecules and clusters.

I. INTRODUCTION

The *ab initio* many-body Green's function ADC methods have been first introduced for calculation of excitation and ionization energies of closed shell species [1, 2] and since then generalized for the description of double [3] and triple [4] ionization energies. The ADC(n) schemes of various orders (n) are size consistent and compact relative to the corresponding truncated CI expansions [5]. While initially developed within the many-body Green's function approach, the ADC can be reformulated as wave-function method using the intermediate state representation (ISR) [6, 7]. This has led to applications of the ADC-ISR technique to calculation of properties of and transition moments between excited [7], singly ionized [8] and doubly ionized [9] bound states. Recently, it has been shown that the ADC schemes in conjunction with iterative block-Lanczos (BL) diagonalization [10–12] and the Stieltjes-Chebyshev moment theory [13] can be used also for accurate and efficient characterization of bound-continuum transitions, i.e. for calculations of the decay widths of resonance states [14] and photoionization cross-sections [15–17]. In the bulk of the ADC work cited above, Gaussian type orbitals (GTOs) have been used as a single-electron basis as is indeed customary in the *ab initio* quantum chemistry. However, a very recent benchmark study [16] indicates that it is the use of the GTOs in the excitation ADC schemes that leads to the onset of major inaccuracies in molecular photoionization cross-section calculations at about 70 eV above threshold. This trend has been shown to be general for a series of molecular species and independent of the order of the employed ADC scheme [16]. Moreover, GTO-based ADC-Lanczos-Stieltjes method fails to reproduce not only the narrow features of the cross-section due to excitation resonances (as is fully expected of a moment theory technique), but even the much broader features, such as Cooper minima, e.g. in argon photoionization. Very similar behaviour has been observed in a recent implementation of the GTO/Stieltjes approach within linear response coupled cluster models for electronic excitations [18]. Even very careful GTO selection cannot afford converged high order moments, i.e high energy features and high resolution, without running into linear dependence problems [18]. The inadequacy of the GTO bases for the characterization of the molecular photoionization calls for an introduction of new basis sets, better suited for the description of the oscillatory continuum

wave functions across the interaction region. Several such basis sets have been already introduced in the nineties within the framework of the many-body methods that do not fully include double electronic excitations and were successfully used for the solution of the time-independent many-electron problems, e.g. for photoionisation cross-section calculations, see e.g. Ref. [19]. The present work addresses the single-electron basis set issue by construction of ADC schemes explicitly treating not only single [ADC(1)], but also double [ADC(2)] excitations and applying them to the solution of both time-independent and time-dependent many-electron problems. The employed single-electron basis is composed of the spherical harmonics for the angular part and a B-spline expansion for the radial coordinate.

B-splines [20] are one-variable piecewise polynomial functions designed to generalize polynomials for the purpose of approximating arbitrary functions on some interval $[0, R_{max}]$. They have the property of approaching completeness as much as desired by refining the corresponding knot sequence, i.e. the set of points that divides the full interval into sub-intervals [20]. B-spline basis is known to lead to negligible linear dependences even for large bases (i.e. dense knot sequences), and are computationally competitive with the "local" finite-difference methods [21]. Moreover, the use of such a pre-determined quasi-complete set of one-particle orbitals eliminates the need of any a priori procedure in selecting the parameters for the Gaussian-type or Slater-type functions required in the standard L^2 quantum chemistry calculations which often depend upon non-trivial treatment to minimize the linear dependence embedded in the choice of basis functions. This accounts for the extensive use of B-splines in atomic and molecular calculations [20, 22, 23].

This article is organized as follows. The relevant aspects of the ADC approach to excited states are presented in Sec. II. A generic description of the B-spline basis set properties is given in Sec. III. Computational details regarding the effective implementation within the ADC schemes, are discussed in Sec. IV. Sec. V is devoted to the testing of the proposed technique through calculation of a series of atomic total photoionization cross sections, while in Sec. VI we present the first application to time-dependent problems through calculation of the high-order harmonic generation (HHG) spectra of Ar atom in strong IR field. Conclusions and prospectives are given in Sec. VII.

II. ADC *AB INITIO* SCHEMES WITHIN THE INTERMEDIATE STATE REPRESENTATION

The ADC schemes for excited states of closed-shell systems were originally derived as approximations to the polarization propagator, based on an algebraic reformulation of its diagrammatic perturbation theory. The ADC(n) polarization propagator is complete up to order n of perturbation theory in the electron interaction and includes also higher-order diagrams in the form of infinite partial (incomplete) summations [2]. ADC was later recognized [6] as being interpretable as a wave-function method as well. In fact, it establishes a connection between propagator and wave-function methods. The latter interpretation comes from the explicit construction of the intermediate states representation (ISR) that gives rise to the ADC form of the propagator, providing an alternative approach to the hierarchy of the ADC schemes [6, 7]. The starting point is the construction of the so called correlated excited states (CES), defined as

$$| \Psi_I^0 \rangle = \hat{C}_I^\dagger \mid \Psi_0 \rangle \,, \tag{1}$$

where the operators $\hat{C}_I^\dagger$ denote the physical excitation operators corresponding respectively to 1p1h, 2p2h, etc. excitations,

$$\hat{C}_I^\dagger = \left\{ \hat{a}_a^\dagger \hat{a}_i \,;\, \hat{a}_a^\dagger \hat{a}_b^\dagger \hat{a}_j \hat{a}_k \;\; (a<b, j<k) \ldots\ldots \right\} , \tag{2}$$

and $| \Psi_0 \rangle$ is the exact correlated ground state of the system.

This non-orthogonal CES basis set is complete in the space of the excited states of the N-electron system [24] and has the advantage that ground state correlation is already built into every basis vector. It can be orthonormalized in a two-step procedure. First, one performs Gram-Schmidt orthogonalization of each excitation class with respect to all the lower excitation classes. The states $| \Psi_y^{m\#} \rangle$ formed in this first step are referred to as precursor states. The second step is symmetric orthonormalization of the resulting precursor states within each excitation class. As an example the procedure for the first (1h1p) excitation class gives the following precursor states:

$$| \Psi_{ai}^{1\#} \rangle = \hat{a}_a^\dagger \hat{a}_i \mid \Psi_0 \rangle - \mid \Psi_0 \rangle \langle \Psi_0 \mid \hat{a}_a^\dagger \hat{a}_i \mid \Psi_0 \rangle \,. \tag{3}$$

The second step gives

$$| \tilde{\Psi}^1_{ai} \rangle = \sum_{bj} | \Psi^{1\#}_{bj} \rangle \left(S^{-\frac{1}{2}} \right)_{bj,ai} , \tag{4}$$

where **S** is the overlap matrix of the first excitation class precursor states, i.e.

$$S_{bj,ai} = \langle \Psi^{1\#}_{bj} \mid \Psi^{1\#}_{ai} \rangle \tag{5}$$

In a compact notation the excitation class orthogonalized (ECO) states can be written as

$$| \tilde{\Psi}^m_x \rangle = \hat{Q}^{m-1} \sum_y | \Psi^m_y \rangle \left(S^m_{yx} \right)^{-1/2} , \tag{6}$$

where S^m_{yx} is defined as

$$S^m_{yx} = \langle \Psi^m_y \mid \hat{Q}^{m-1} \mid \Psi^m_x \rangle \tag{7}$$

and

$$\hat{Q}^m = \hat{1} - \sum_{l=0}^{m} \hat{P}^l \tag{8}$$

is the projector operator onto the space orthogonal to the first m excitation classes. Finally, every intermediate state can be expressed as

$$| \tilde{\Psi}_I \rangle = \tilde{C}^\dagger_I \mid \Psi_0 \rangle , \tag{9}$$

where all the effects of the consecutive orthonormalizations are encoded in the new creation operators $\tilde{C}^\dagger_I$.

The ADC secular matrix is the representation of the shifted electronic Hamiltonian operator $\hat{H} - E_0$ in the ECO-CES space:

$$\mathscr{H}_{IJ} = \langle \tilde{\Psi}_I \mid \hat{H} - E_0 \mid \tilde{\Psi}_J \rangle = \langle \Psi_0 \mid \tilde{C}_I \left[\hat{H}, \tilde{C}^\dagger_J \right] \mid \Psi_0 \rangle . \tag{10}$$

At this point Møller-Plesset (MP) perturbation theory is introduced to describe the ground state correlation, i.e. $| \Psi_0 \rangle$ and E_0:

$$| \Psi'_0 \rangle = | \Phi^{HF}_0 \rangle + | \Psi^{[1]'}_0 \rangle + | \Psi^{[2]'}_0 \rangle + | \Psi^{[3]'}_0 \rangle + \ldots , \tag{11}$$

where the first order correction $|\,\Psi_0^{[1]'}\rangle$ contains only double excitations (2h2p) with respect to $|\,\Phi_0^{HF}\rangle$, while $|\,\Psi_0^{[2]'}\rangle$ contains single, double, triple and quadruple excitations.

The vertical excitation energies are obtained by solving the eigenvalue problem $\mathbf{HV} = \omega\mathbf{V}$, and the excited eigenstates of the system are therefore given in the basis of the intermediate states:

$$|\,\Psi_n\rangle = \sum_I V_{I,n}\,|\,\tilde{\Psi}_I\rangle\,. \tag{12}$$

Using this explicit expression for the excited states of the system, one contains the corresponding transition moments as

$$\langle\Psi_m\,|\,\hat{D}\,|\,\Psi_0\rangle = \mathbf{V}_m^\dagger\cdot\mathbf{F} = \sum_{rs} d_{rs}\mathbf{V}_m^\dagger\cdot\mathbf{f}_{rs}\,, \tag{13}$$

where d_{rs} are the matrix elements of the dipole operator on the one particle orbitals chosen as basis set functions. The matrix of effective transition amplitudes $\mathbf{f}$ and the associated vector $\mathbf{F}$ are defined by:

$$f_{I,rs} = \langle\tilde{\Psi}_I\,|\,\hat{a}_r^\dagger\hat{a}_s\,|\,\Psi_0\rangle\,,\quad F_I = \langle\tilde{\Psi}_I\,|\,\hat{D}\,|\,\Psi_0\rangle\,. \tag{14}$$

The hierarchy of ADC(n) approximations is obtained for each order n by truncating the intermediate state manifold at some limiting excitation class and, also, by truncating the resulting perturbation expansions for the included classes in the way consistent with the polarization propagator approach. For example, at the ADC(2) level, the Hamiltonian matrix of the system can be represented as

$$\mathscr{H}^{\mathrm{ADC}[2]} = \mathscr{H}^{[0]} + \mathscr{H}^{1,1[1]} + \mathscr{H}^{1,1[2]} + \mathscr{H}^{1,2[1]} + \mathscr{H}^{2,1[1]} \tag{15}$$

where $\mathscr{H}^{i,j[N]}$ denotes the ipih-jpjh excitations block of the Hamiltonian computed at the order N of perturbation theory.

Thus, in ADC(2) the perturbation expansion of the secular matrix elements extends through second, first and zero-th order in the 1h1p block, the 1h1p-2h2p coupling block and the diagonal 2h2p block, respectively. In a similar way the 1h1p and 1h2p parts of the effective transition amplitudes are given by perturbation expansions through second and first order respectively.

The ADC(n) schemes are size consistent and compact relative to the corresponding truncated CI expansions [5]. In the ADC(1) scheme the Hamiltonian reduces to the configuration interaction singles (CIS) one, while the transition moment with respect to the ground state are improved and are expressed as

$$\langle \tilde{\Psi}_i^a \mid \hat{D} \mid \Psi_0 \rangle = d_{ai} + \sum_v \sum_o \frac{\langle va \mid\mid oi \rangle}{\varepsilon_o + \varepsilon_i - \varepsilon_v - \varepsilon_a} d_{ov} \tag{16}$$

where $\langle va \mid\mid oi \rangle$ is the antisymmetrized two-particle Coulomb integral in physicists' notation and the two indices v and o run over the virtual and the occupied canonical (Hartree-Fock) orbitals respectively. Therefore ADC(1) can be already considered as an improved version of CIS.

III. B-SPLINE BASIS SET

Monocentric B-spline basis is composed of a spherical harmonics for the angular part and B-splines for the radial coordinate. Single particle orbitals are therefore expressed as

$$\psi_{ilm} = \frac{1}{r} B_i(r) Y_{lm}(\theta, \phi) \tag{17}$$

The use of B-splines in the atomic problem has been pioneered by Shore [25] and employed in the atomic and molecular context by several authors [22]. In particular, B-splines are able to provide a very accurate representation of continuum states, which makes them superior to more conventional $\mathscr{L}^2$ basis sets. Although the first applications were to static properties, it has turned out that B-splines perhaps are even more important for the calculation of dynamic properties such as multiphoton excitation, above-threshold ionization (ATI) and HHG in atoms [26].

Splines are functions designed to generalize polynomials for the purpose of approximating arbitrary functions. B-splines are piecewise polynomial functions, of order k completely defined given the order and a set of points (knot sequence) which may be in part coincident, and divide the radial interval $[0, R_{max}]$ into adjacent subintervals:

$$0 = t_1 \leq \ldots \leq t_n = R_{max}\,. \tag{18}$$

Each different point belonging to the knot sequence is usually called a breakpoint and denoted by ξ_i.

The first step in our calculations is the solution of the discretized closed-shell Hartree-Fock equations,

$$\hat{h}^{HF}\psi_n = \varepsilon_n \psi_n \,, \tag{19}$$

where $\hat{h}^{HF}$ is the spin-free ground-state Fock operator of the neutral system,

$$\hat{h}^{HF} = \hat{h}_0 + \sum_{occ} (+2\hat{J}_{occ} - \hat{K}_{occ}) \,. \tag{20}$$

In the molecular case Eq. (19) is solved for every irreducible representation of the molecular point symmetry group, and the expansion of the wavefunction ψ_n contains all the angular functions belonging to the particular irreducible representation. In the atomic case, the HF equations can be projected upon the l-m spherical harmonic subspace and they simplify in the following way

$$\hat{h}_l^{HF}\psi_{lm,n}(r) = \varepsilon_{l,n}\psi_{lm,n}(r) \,. \tag{21}$$

The evaluation of the B-spline radial two-electron integrals is carried out by direct two- dimensional numerical integration as reported in [27].

Solving Eq. (19) self-consistently, we obtain a quasi-complete set of discretized one-particle functions $\psi_{lm,n}$ corresponding to electronic orbitals with an orbital angular momentum l and variable energy (both negative and positive) defined by the Hartree-Fock effective one-particle Hamiltonian. We therefore obtain the set of occupied HF orbitals and the full orthogonal complement of virtual orbitals, expressed in terms of B-spline basis functions. These canonical orbitals are then used to construct the ADC many-body Hamiltonian. We therefore do not work directly with primitive B-splines and as a consequence we perform the one- and two-electron integral transformation from the original B-spline basis to the HF basis set. The computational details are given in Sec. IV. Since ADC is formulated as a perturbative theory with respect to the HF mean-field Hamiltonian, the canonical ADC(n) formulae are valid only in terms of HF orbitals. Apart from the case of the first order ADC(1) level of theory, they become much more complicated if a different orbital set is used.

The B-spline knot sequence we use is the parabolic-linear sequence, which is a mix of these two types of sequences: a short-range dense one which concentrates points near the nucleus with

quadratically increasing knot spacing and a linear knot spacing sequence for larger values of r necessary for continuum states description. The range of kinetic energies accurately described by the B-spline basis set can also be tuned changing the knot spacing in the linear region. The connection between the two regions is made at an intermediate radial distance r_0, imposing continuity of the breaking point function ξ_i and of its first derivative. The explicit parabolic-linear knot sequence formula is:

$$\xi_i = \alpha(i-i_0)^2 \; for \; 1 \leq i < i_0 \qquad (22)$$
$$\xi_i = h(i-i_0) \; for \; i_0 \leq i \leq n$$

The intermediate radius is defined by the index i_0 in the following way $r_0 = \xi_{i_0} = \frac{r_{max}(i_0-1)}{2n-i_0-1}$ and the quadratic and linear coefficients by $\alpha = \frac{r_0}{(i_0-1)^2}$ and $h = \frac{r_{max}}{(n-i_0)}$ respectively.

The explicit basis sets used in this work are listed in Table I. The B-spline Set 3 is represented graphically in Fig. 1.

IV. COMPUTATIONAL DETAILS

The number of basis functions used in B-spline ADC is well above the standards of a typical *ab initio* calculation and as a result, the numerical algorithm has to be highly optimized. Consequently, it becomes necessary to take advantage of the parallel computing environment [28, 29] which has become increasingly easy to manage.

While our choice of the single-particle basis functions leads to higher computational effort than in the GTO case, it at the same time simplifies tremendously the numerical algorithm mainly because of the absence of linear dependencies to take care of; moreover, the minimal localized support of the individual primitive B-spline basis functions allows to reduce the number of B-spline one-electron and two-electron integrals to be calculated and stored at the beginning of the calculation. However we want to mention that in general, although the MPI technology allows to substantially reduce the memory requirement per single-node, substantial global amount of RAM (spread across a high number of nodes) is still needed for B-spline ADC calculations requiring a big dimension of the one-electron basis set expansion.

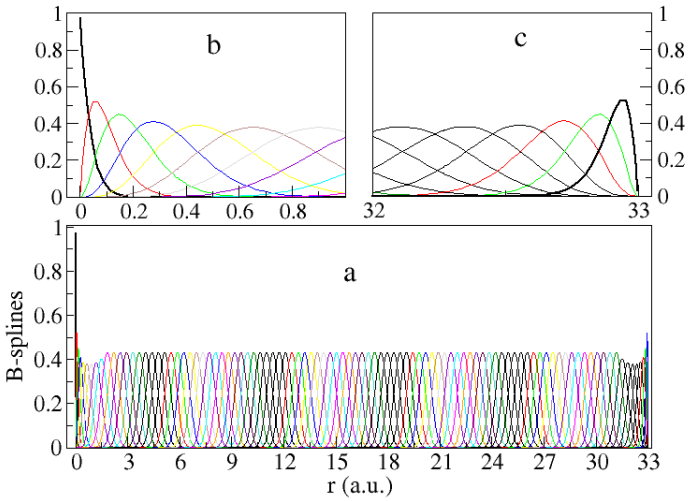

Figure 1: a – graphical representation of B-spline basis Set 3, with $R_{max} = 33$ a.u.; the knot sequence is linear and the total number of B-spline functions is 97. b – magnification of the B-spline functions in the radial region close to the origin. c – magnification of the B-spline functions in the radial region close to the box boundary.

The numerical procedure required in a B-spline-ADC calculation consist of four key steps, namely:

1. Solution of the B-spline HF equations.

2. One- and two-electron integral transformations with simultaneous calculation of the first order Hamiltonian and dipole matrix-elements on the fly.

3. Calculation of the second-order matrix elements in the ADC(2) method.

4. Full/iterative diagonalization of the ADC Hamiltonian and calculation of the static physical quantity of interest (e.g. a cross-section) via the SI technique or time-propagation of an initial state in order to obtain the dynamic quantity of interest (e.g. HHG spectrum).

The first step consists of solving a set of one-particle integro-differential equations with non-local terms, i.e. the Hartree-Fock equations. These equations are solved iteratively, in each irreducible representation of the electronic Hamiltonian, in the standard way [30].

The second step makes the integrals transformation from the primitive B-spline basis set to the basis of the Hartree-Fock orbitals. The transformation is performed with the common four-step algorithm, giving a scaling of N^5 with respect to the number of orbitals to be transformed. Because of the number of basis functions involved, both the memory requirements and the time of the transformation can quickly become unaffordable with the increase of the number of spherical harmonics and/or of the radial B-spline functions used in the monocentric expansion (Eq. (17)). We approach this problem by calculating only the two-electron integral types required by the ADC Hamiltonian and dipole matrix elements: in the ADC(1) case only the integrals involving two virtual canonical orbitals indices are needed, namely integrals of the type (vv|oo) and (vo|vo). In the ADC(2) calculations two other types of integrals are required, namely the (vv|vv), (vv|vo) and the less demanding (vo|oo) types [2].

We furthermore make use of the Hamiltonian symmetry group to divide every type of integral calculation with respect to the quadruplet of orbital irreducible representations involved. In the general molecular case we use the biggest Abelian molecular symmetry subgroup, while in atomic calculations we exploit the full rotational symmetry. Following this strategy we end up with an increased number of less demanding single calculations to be performed. Each of these reduced single calculations has been massively parallelized, both inter-nodes, with the standard MPI (message passing interface) technology in parallel computing environment, and intra-node with the OpenMP (shared memory) technology.

A schematic representation of the way every specific quadruple of two-electron integrals undergoes the 4-indices transformation in parallel is given in Fig. 2. In details, since the first transformation step, the two-electron integral vector memory allocation is divided between the computational MPI nodes available. This division is performed onto the first index of the four-indices two-electron integral tensor V_{IJKL}. Each of these pieces of the two-electron integral vector undergoes the four indices transformations from V_{IJKL} to V_{PQRS} locally on every node in parallel, and only after the last index transformation is performed the resulting fully transformed partial vectors from every node are sent to a specific node where they are summed together. The advantage of this algorithm is that it turns out to never be necessary, at any intermediate stage of the transformation, to have the full integral vector dynamically allocated on a single node.

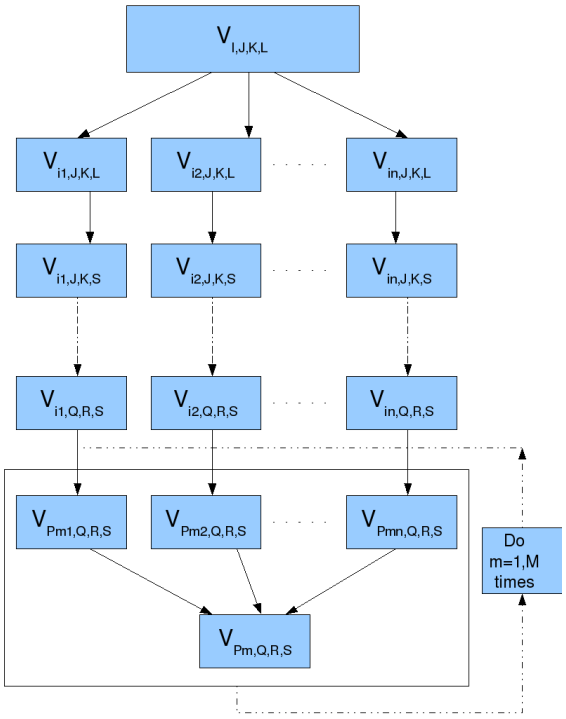

Figure 2: Schematic representation of the way the two-electron integral transformation is parallelized. The indices I,J,K,L refer to the primitive basis functions of Eq. (III); the indices P,Q,R,S refer to the Hartree-Fock canonical orbitals.

Moreover, even if the full final transformed integrals vector can be bigger than the full partially transformed intermediate ones, it's complete allocation onto a single node is not required because it can be computed pieces by pieces sequentially. The contributions to the first order matrix elements of the ADC Hamiltonian and of the ADC transition moments are calculated on the fly at the last step of the integral transformation. The integrals involved in the second-order ADC matrix elements are instead stored on disk. The OpenMP technology is used to parallelize every intermediate transformation performed on every node, reducing therefore considerably the time of the computation.

The third step, in the case of the ADC(2) level of theory, evaluates the remaining terms of the ADC Hamiltonian matrix and transition moments using the relevant two-electron integrals

stored on disk. The matrix we deal with in ADC(2) are of a size often up to 1,000,000 or greater. In ADC(1) the linear scaling with respect to the number of basis functions is however much more favourable. The value of the individual matrix element, which at the first order ADC(1) level represents a two-variable integral over a two-body Coulomb interaction is in general small but non-zero and, as a result, the matrix is non-sparse. At the second order level the 1h1p-2h2p coupling block is quite sparse, around 10/15%, while the 2h2p block is diagonal; this simplifies enormously the computation and actually makes such types of calculation possible.

The calculation is performed by dividing the matrix into a large number of sub-matrices of a size storable on a single node. Every sub-matrix is calculated in parallel, with every node computing a partial contribution to it. The same process is repeated for every sub-matrices, the number of times this is done depending on the memory storage capabilities available and on the matrix dimension. Therefore for memory reasons the different sub-matrices are calculated sequentially one after the other, even if they are independent one of each other. Nevertheless the extension to the parallel computing environment speeds up substantially this step as well, because every node just calculates its own specific contribution to the given sub-matrix and moreover this calculation is OpenMP parallelized as well.

The fourth step involves the extraction of the relevant physical information from the ADC Hamiltonian. In the particular case of a total cross-section calculation, performed using the SI technique, we are interested in the pseudospectrum of the Hamiltonian and in the transition moments of the pseudo-eigenstates. A newly implemented, parallelized, BL diagonalization routine allows us to obtain a limited number of energy eigenvalues and their corresponding eigenvectors by diagonalizing the ADC(2) sparse matrices generated in the third step. A direct diagonalization is instead performed in the ADC(1) calculations presented here. This is possible because with the B-spline basis sets used the ADC(1) matrices have typically small enough dimension, being for example 1978 in our calculation of krypton atom. The range of the B-spline and spherical harmonics expansions over which such a full diagonalization procedure is still applicable, is quite large for the ADC(1) Hamiltonian, because of the linear scaling of its dimension with respect to the number of one-electron basis functions. Finally, given the pseudospectrum, it is possible to calculate the transition amplitudes and ultimately the cross

section. This latter calculation can be performed on any single-node CPU. In the case of the dynamical calculation, the time-dependent Schrödinger equation (TDSE) in the basis of the ADC intermediate states is solved via the Arnoldi-Lanczos algorithm. More detail on the time-dependent method will be reported in a subsequent work.

V. ATOMIC PHOTOIONIZATION CROSS-SECTIONS BY COMBINATION OF B-SPLINE-ADC AND STIELTJES METHODS

Our goal here is to test the accuracy of the newly designed and implemented B-spline ADC method at the ADC(1) and ADC(2) levels of *ab initio* theory for bound-free transitions by calculating a series of total photoionization cross-sections. We use a test set of noble gas atom cross-sections for which both very accurate experimental results and a series of GTO-based calculations are available. Especially the Ar and Kr atoms provide very good test case, because their cross-sections contain structured features, such as the Cooper minimum in argon and the $3d$-channel opening in krypton, which so far has been found to be challenging for the GTO calculations.

As in the case of the GTO calculations [15–17], we use the Stieltjes imaging (SI) technique [13, 15–17] which allows one to extract the correctly normalized oscillator-strength density in the electronic continuum. This also enables us to verify the stability of the B-spline results with respect to the Stieltjes order, providing yet another test of the accuracy of the basis set used and of its ability to reproduce the higher spectral moments. Naturally, the accurate representation of these spectral moments is the key factor responsible for the ability to describe such features as Cooper minima. We quantify the deviation of the ADC(1) and ADC(2) cross-sections from the experimental ones by computing their energy-dependent and energy-averaged relative discrepancies over the covered photon energy region.

The radial B-spline basis set used in our calculations are described in detail in Table I. Figs. 3, 4 show the experimental total photoionization cross section Ref. [31, 32] as well as a series of Stieltjes imaging results obtained via full diagonalization of the ADC(1) Hamiltonian matrix and Lanczos diagonalization of the ADC(2) Hamiltonian matrix, of He and Ne atoms.

Basis set Index	$R_{\max}$ (a.u.)	N_{splines}	Linear Region step h (a.u.)	Quadratic coeff. α (a.u.)	R_0 (a.u.)
Set 1	21.0	45	0.6	0.0295	2.392
Set 2	47.0	87	0.61	0.032	2.595
Set 3	33.0	97	0.367	–	0.0
Set 4	60.0	157	0.4	–	0.0
Set 5	120.0	200	0.6	–	0.0

Table I: B-splines basis sets employed in the calculations; for every basis set the dimension of the discretisation box, the number of B-spline functions and the step in the linear grid region are given.

Checking the convergence with the maximal angular momentum of the spherical harmonics basis, we have found it generally sufficient, as expected for the one-photon absorption processes described in this paper, to truncate the angular expansion at values of $L_{\max}$ corresponding to $L_{\max}^{occ}+1$, where $L_{\max}^{\text{occ}}$ is the maximum angular momentum of the occupied orbitals. In the case of He, the results presented are the one for the $L_{max}=2$ spherical harmonics expansion, while for Ne atom the spherical harmonics expansion used extends up to $L_{\max}=3$. In the ADC(2) Ne calculations, $1s$ orbital was frozen in both the singly and the doubly excited intermediate states. We have chosen the starting vectors for the BL scheme to be the unit vectors corresponding to selected 1h1p intermediate states with the transition moment from the ground state bigger than a fixed threshold value. Throughout this work, we report the B-spline ADC(2)cross-sections converged with respect to the number of Lanczos iterations.

One can see that the agreement between the experimental and the theoretical cross sections improves with the order of the ADC scheme. The highest-order ADC(2) result for He essentially coincides with the experimental one apart from the 2snp ^1P auto-ionization resonance region around 60 eV. In the Ne calculation the ADC(1) result shows a displacement of the main peak of about 5 eV, consistently with the GTO ADC calculation of Ref. [15]. The ADC(2) result shows a good agreement with the experiment. As expected, in the Ne case as well, the use of SI leads to disagreement between the ADC(2) cross-section and the experimental one in the autoionization resonance region around 45.5 eV due to the 2s-np autoionizing states. This inability of the Stieltjes-Chebyshev moment theory to reproduce very sharp spectral features is well known and apparently persists also in the B-spline implementation.

ab initio level	He	Ne	Ar	Kr	average
ADC(1)	6.2 %	12.0 %	11.6 %	7.9 %	9.4 %
ADC(2)	2.5 %	7.5 %	8.1 %	6.0 %	6.0 %

Table II: Relative deviations of the B-spline ADC-Stieltjes photoionization cross-sections from the experimental results of Ref. [32] across the energy range of ionization threshold to 170 eV.

At a first glance, the B-spline results have comparable accuracy to the one obtained in Ref. [15] with the GTO-based ADC; however, if one looks carefully at the high energy tail of the cross-section, a much better agreement with the experiment is obtained with the B-spline basis set. Details of this analysis are given in Fig. 5. The discrepancy in the Gaussian based calculation arose from the inability of the Gaussian basis to provide a correct description for strongly oscillating continuum states as well as for high Fourier components of the ground state wave function [16]. B-splines completely fix this error and give accurate cross-sections up to arbitrary values of the energy, depending on the spatial density on knots used, see discussion in Sec. III. Average relative deviations of the computed He and Ne cross-sections from the experimental ones are given in Table II.

Argon photoionization cross-section is of particular interest for testing the accuracy of our method due to the presence of the Cooper minimum that is known to present a challenge for the GTO calculations. In Fig. 6 the B-spline ADC(1) and ADC(2) theoretical photoionization cross sections of Ar up to 40 eV of photon energy are presented, together with the experimental results of Chang *et al.* [33] and the most recent one of Samson *et al.* [32]. The B-spline basis set parameters used for this calculations are given in Table I. The spherical-harmonics expansion extends up to $L_{max} = 3$. In the ADC(2) Ar calculations, we have frozen the core $1s$, $2s$ and $2p$ orbitals in both the singly and doubly excited intermediate configurations. We therefore allow only the valence holes in the 1h1p and 2h2p state manifold. One can see that the agreement between the experimental and the theoretical cross sections improves with the order of the ADC scheme. The overall behaviour of the cross-section is very well reproduced with B-splines and the peak position is well reproduced even at the ADC(1) level. The ADC(2) curve, on the other hand, matches better with the experimental data in the energy region from

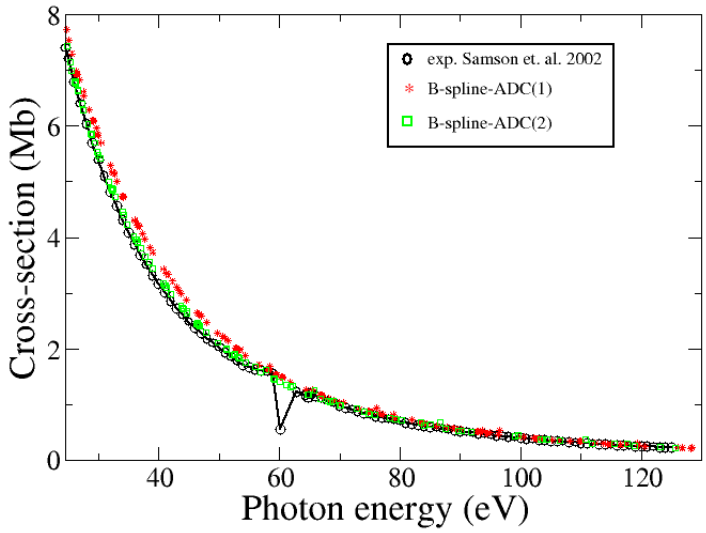

Figure 3: Total photoionization cross-section of He atom. Circles – experimental result of Ref. [32], stars – B-spline-ADC(1) result, from Stieltjes order 5 to 34; squares – B-spline-ADC(2)-Lanczos-Stieltjes cross-section, using the Stieltjes orders 5 to 34. Basis set 2 was employed (see Table I). With this basis set, the ADC(1) and ADC(2) matrices for He have the dimensions of 88×88 and 96500×96500 respectively. The ADC(2) results was obtained using BL pseudospectrum of 3960 eigenvalues and eigenvectors.

the 3s ionization limit at 28 eV up to 40 eV. The 3s ionization limit, which is characterized by the accumulation of autoionization structures starting from 25 eV up to 28 eV is, however, not resolved by our calculations, as in the case of Ne, due to insufficient energy resolution intrinsic to the SI procedure. Average relative deviations of the computed Ar cross-sections from the experimental ones are given in Table II.

Fig. 7 shows the total photoionization cross section of Ar in the region of the Cooper minimum [34]. The Lanczos convergence of the Cooper minimum shape has been more difficult in this energy region, and it has been reached only after almost 30000 iterations. Both ADC(1) and ADC(2) models reproduce the shape of the minimum, with the ADC(2) providing a better quantitative agreement with the experiment in terms of the Cooper minimum position. In fact, ADC(2) gives an almost perfect prediction of the position of the Cooper minimum at 49 eV,

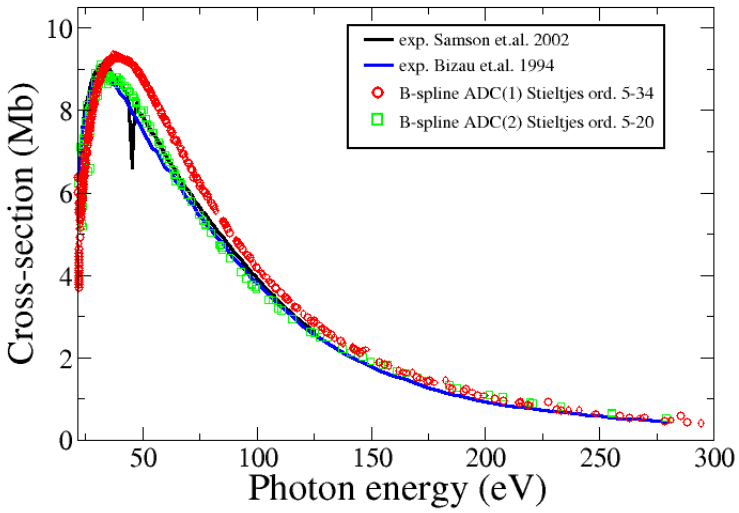

Figure 4: Total photoionization cross-section of Ne atom. Full red line – experimental result of Ref. [32], full blue line – experimental result of Ref. [31], circles – B-spline-ADC(1) result, Stieltjes orders 5 to 34; squares – B-spline-ADC(2)-Lanczos-Stieltjes cross-section, Stieltjes orders 5 to 20, obtained using BL pseudospectrum of 26000 eigenvalues and eigenvectors. Basis set 2 was employed (see Table I). With this basis set, the dimensions of the ADC(1) and ADC(2) matrices are respectively 472×472 and 379970×379970.

while the ADC(1) predicted value is at about 53 eV. The position of the following maximum at 79 eV is overestimated by almost 4 eV from the ADC(1) calculation, while it is underestimated by the nearly the same amount from the ADC(2) one. As it is possible to notice the ADC(1) result is overall closer to the experimental result by Samson et. al. [32], while the ADC(2) curve is closer to the experimental result by Chang et. al. [33]. Both results are also in good agreement with the B-spline TDLDA theoretical calculations in [35], in which the correct normalization of the final continuum states was performed.

It is worth noting that the Cooper minimum is due to a change of sign of the radial dipole matrix elements, which pass through zero at a certain energy [34], and therefore it is already tractable within one-electron models such as the simple SAE (single active electron approach),

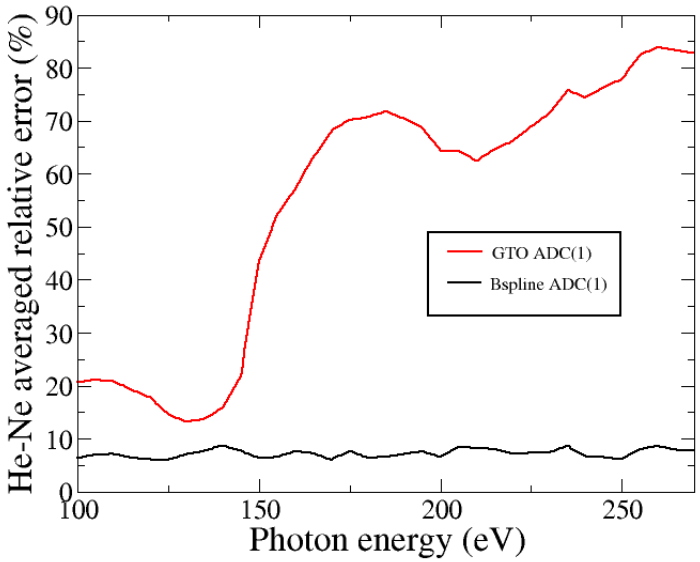

Figure 5: Relative deviations of the calculated ADC-Stieltjes photoionization cross-sections, averaged over Ne and He atoms, from the experimental result, as a function of the energy in the high energy range, i.e. between 100 eV and 250 eV. Black full line – B-spline-ADC(1)-Stieltjes result, red full line – GTO-ADC(1)-Lanczos-Stieltjes result.

as has been verified within LDA in [35], although its precise energy position may be sensibly influenced by correlation effects. Moreover the possibility of describing properly the Cooper minimum feature is strongly related to the ability of the basis set to properly represent the continuum oscillating single-electron orbitals or, in other words, on the accuracy of the basis set in giving good representation of high order spectral moments in the Stieltjes imaging framework. In Fig. 8 a series of Stieltjes approximations of various orders based on the B-spline ADC(1) and ADC(2) calculation as well as the GTO-based ones are shown for direct comparison. The GTO basis used is the fully uncontracted cc-pCVQZ augmented with 5s7p7d4f KBJ continuum exponents [36]. Importantly, the GTO basis calculation fails completely in this case, in contrast to the present B-spline based one. Clearly, the B-spline calculation shows a very good stability of the Stieltjes orders, in contrast to the GTO calculation in which no convergence of the SI procedure can be detected. This, of course, comes at the expense of the much larger size of the

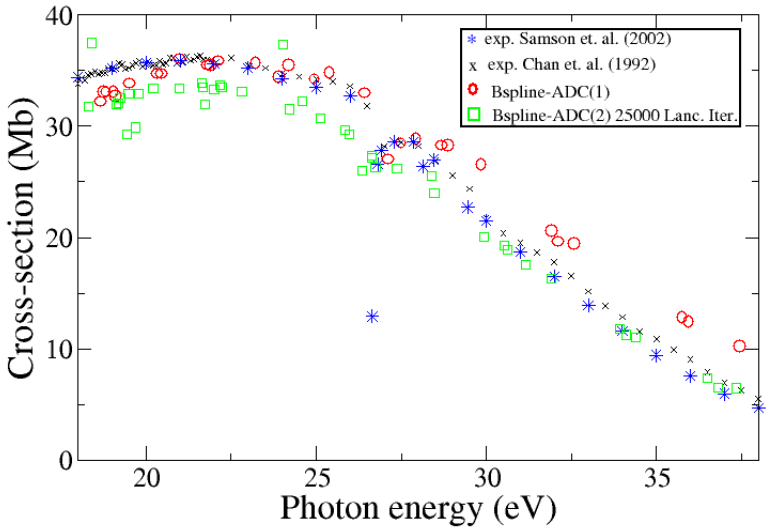

Figure 6: Total photoionization cross-section of Ar atom. Stars – experimental result of Ref. [32], crosses – experimental result of Ref. [33], circles – B-spline-ADC(1) result, Stieltjes orders 5 to 18; squares – B-spline-ADC(2)-Lanczos-Stieltjes cross-section, Stieltjes orders 5 to 18, obtained using BL pseudospectrum of 10000 eigenvalues and eigenvectors. Basis set 1 was employed (see Table I). With this basis and excitation restrictions, the ADC(1) and ADC(2) matrices have dimension of 602×602 and 396541×396541, while the size of the BL pseudospectrum for which the cross-sections convergence is obtained is 10000.

B-spline basis that is free of the linear dependency problem.

The accuracy of the B-spline basis set to represent the continuum functions within the interaction volume makes it possible to correctly reproduce many high order spectral moments. The immediate consequence of this is that a considerable number of Stieltjes orders becomes reliable and as a result, the energy resolution is incredibly improved. In Fig. 9 we show how the Stieltjes orders converge towards the Cooper minimum in argon; as it is possible to see, low orders smooth out the minimum because of the insufficient resolution while high orders correctly reproduce it.

Fig. 10 shows the ADC(1) and ADC(2) theoretical photoionization cross section of Kr in the energy range from 14 eV to 50 eV, together with the experimental results of Chang *et al.*

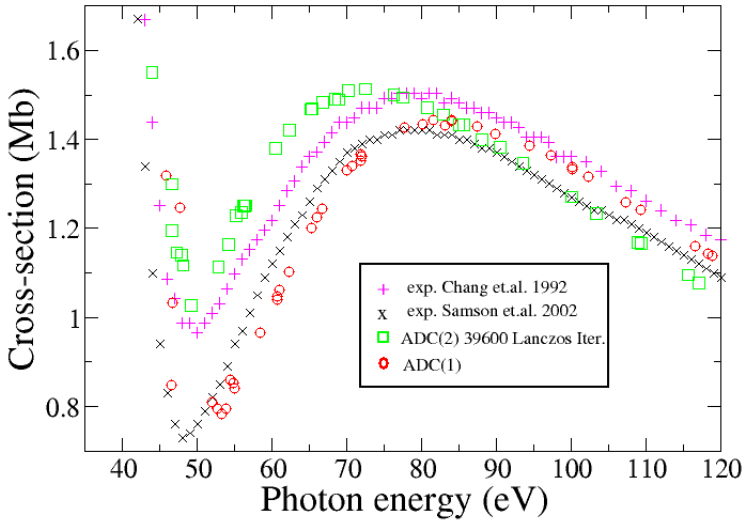

Figure 7: Total photoionization cross-section of Ar atom. Crosses – experimental result of Ref. [32], pluses – experimental result of Ref. [33], circles – B-spline-ADC(1) result, Stieltjes orders 25 to 34; squares – B-spline-ADC(2)-Lanczos-Stieltjes cross-section, Stieltjes orders 25 to 34. The BL pseudospectrum for which the cross-sections convergence is obtained is 30000.

[33] and the most recent ones of Samson *et al.* [32]. The B-spline basis set parameters used for this calculations are given in I. The spherical-harmonics expansion extends up to $L_{max} = 3$ both in the ADC(1) and in the ADC(2) cases. In this ADC(2) Kr calculation, we have frozen, in both the singly and the doubly excited intermediate configuration states, the $1s$, $2s$, $3s$ and $2p$,$3p$ and $3d$ orbitals. We therefore allow single excitations and double excitations just from the $4s$ and $4p$ valence orbitals. This is enough to describe the outer valence energy region (from the ionization threshold to 80 eV) completely at the ADC(2) level. As in the case of argon, the overall behaviour of the cross-section is very well reproduced with B-spline ADC(1), even if the position of the peak is shifted to higher energy with respect to the experimental one, by about 2 eV. As we have already shown using the GTO calculations [16] this is a general feature of the ADC(1) level of theory that overestimates the final state energies. The decreasing behaviour

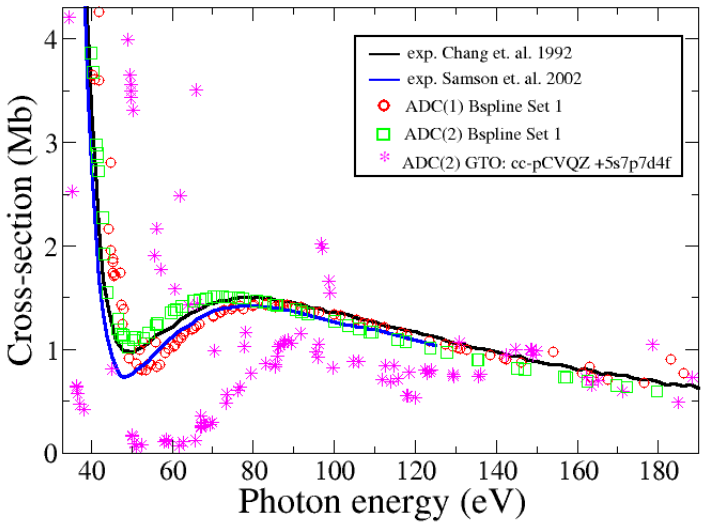

Figure 8: Total photoionization cross-section of Ar atom. Full red line – experimental result of Ref. [32], full black line – experimental result of Ref. [33], circles – B-spline-ADC(1) result, from Stieltjes orders 18 to 34; squares – B-spline-ADC(2)-Lanczos-Stieltjes cross-section, from Stieltjes orders 18 to 34, obtained using BL pseudospectrum of 30000 eigenvalues and eigenvectors, stars – GTO ADC(2)-Stieltjes cross-section, from Stieltjes orders 10 to 30.

is correctly displayed by both theoretical curves, but better agreement with the experiment is obtained by the ADC(2) method. Average relative deviations of the computed Kr cross-sections from the experimental one are given in Table II.

Fig. 11 shows the ADC(1) and ADC(2) cross-sections of Kr in a higher energy region which includes three inner ionization limits: $3d$, $3p$ and $3s$. In this ADC(2) Kr calculation, we have frozen, in the doubly excited intermediate configuration states, the $1s$, $2s$, $3s$ and $2p$ and $3p$ orbitals. The interval from $3d$ up to $3p$ ionization is about 100 eV wide and is characterized by an experimental sigmoid shape with a broad maximum just below the $3p$ limit. The theoretical curves in this range have the correct shape, but they are at greater values than the experimental one. Moreover the SI prevents, in this case, the possibility of reproducing the $3p$ and $3s$ channel-

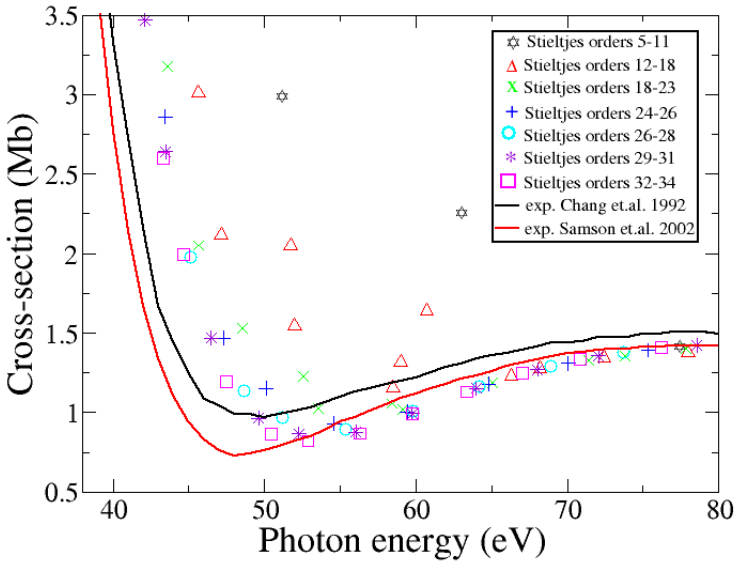

Figure 9: Total photoionization cross-section of Ar atom in the Cooper minimum energy region. Convergence with respect to the Stieltjes order n is shown for a B-spline ADC(1) calculation done with B-spline set 3. Different symbols represent different orders as indicated in the legend. Full red line – experimental result of Ref. [32], full black line – experimental result of Ref. [33].

opening step. At energies above the $3p$ and $3s$ limits the calculations give an almost linear decreasing curve, with a negative slope that correctly reproduces the experimental one.

Finally, let us analyze the relative deviations of the two *ab initio* methods as a function of the photon energy in the same way we have done in [16] for the GTO-ADC calculations. This is done in Fig. 12 where one observes that below 100 eV both ADC(1) and ADC(2) methods lead to impressive agreement with experiment with the relative deviations around 10% and 3% respectively. Moreover, the precision deterioration at higher energies typical of the GTO calculations [16] is not present any more, the average error stabilizing around 5% for both methods.

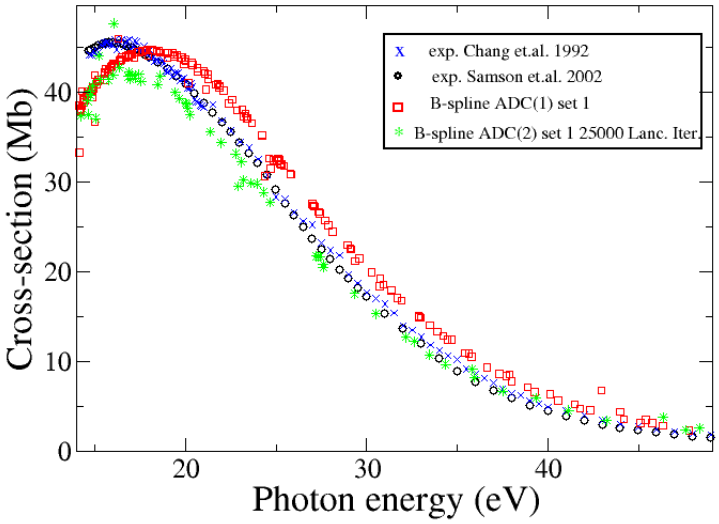

Figure 10: Total photoionization cross-section of Kr atom in the outer valence energy region. Circles – experimental result of Ref. [32], stars – experimental result of Ref. [33]; squares – B-spline-ADC(1) result using B-spline Set 4 (see Table I), from Stieltjes order 5 to 18. With this basis, the ADC(1) and ADC(2) matrices have dimension of 1728×1728 and 1921110×1921110 respectively, while the size of the BL pseudospectrum for which the cross-sections convergence was obtained used is 32000.

VI. HIGH-ORDER HARMONIC GENERATION IN ARGON

In this section we present a first application of the newly implemented B-spline time-dependent (TD) ADC. Here we again concentrate on the effect of the Cooper minimum, since besides its basic importance for photoionization, it also has recently drawn much attention in connection to the HHG by rare gases [37]. Calculation of the HHG spectrum of Ar atom interacting with an intense and short infrared (IR) laser pulse allows us to illustrate the effect of the Cooper minimum on the HHG spectrum by a fully *ab initio* single-atom simulation.

The time-dependent problem is solved within TD-ADC making the following ansatz for the time-dependent electronic wavefunction:

$$|\Psi(t)\rangle = C_0(t)\,|\Psi_0(t)\rangle + \sum_n C_n(t)\,|\Psi_n(t)\rangle \tag{23}$$

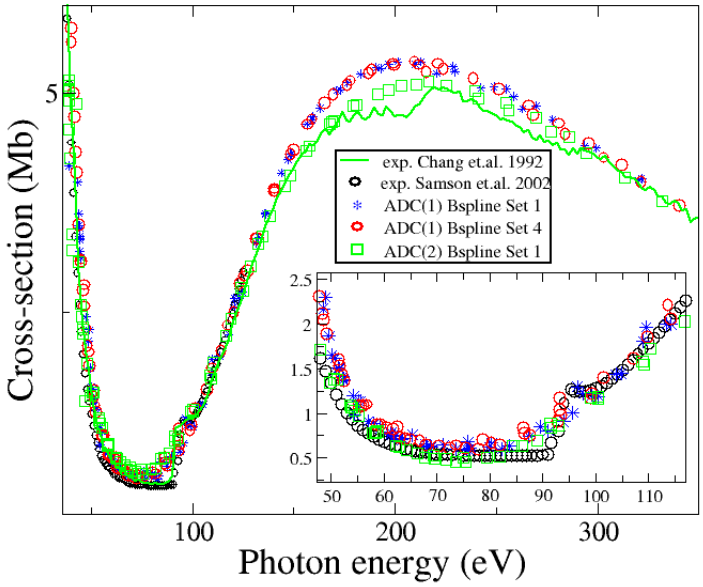

Figure 11: Total photoionization cross-section of Kr atom. Circles – experimental result of Ref. [32], full green line – experimental result of Ref. [33]; stars – B-spline-ADC(1) result using B-spline Set 1, from Stieltjes orders 5 to 34; circles – B-spline-ADC(1) result using B-spline Set 4, from Stieltjes orders 5 to 34; squares – B-spline-ADC(2)-Lanczos-Stieltjes cross-section, from Stieltjes orders 18 to 34, obtained using BL pseudospectrum of 30000 eigenvalues and eigenvectors.

where the coefficients $C_0(t)$ and $C_n(t)$ refer to the ground-state and to the ECO-CES ADC configuration basis states respectively. The time-dependent Schrödinger equation (TDSE) for the unknown coefficients C_0, C_n is solved via the Arnoldi-Lanczos algorithm. More detail on the method will be reported in a subsequent publication [38].

In the following calculation we have used the first-order method of the ADC-hierarchy, namely ADC(1). The HHG spectrum, which is calculated via the expectation value of the electric dipole moment $z(t)$ [39], reads

$$S_{hhg}(\omega) = \frac{1}{20}\frac{1}{3\pi c^3}\left|\int_{-\infty}^{\infty}\left[\frac{d^2}{dt^2}\langle z\rangle(t)\right]e^{-i\omega t}\,dt\,\right|^2 \tag{24}$$

The presented results have been calculated making explicit use of the atomic spherical symmetry. We have used two laser pulses with a carrier frequency $\omega = 0.057$ a.u. (800 nm), a full

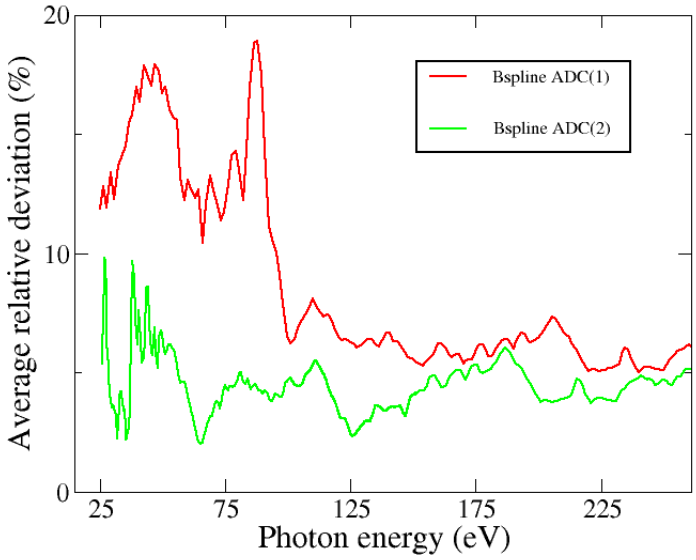

Figure 12: Relative deviations of the B-spline-ADC-Stieltjes photoionization cross-sections from the experimental results averaged on the four closed shell atoms calculated, namely He, Ne, Ar and Kr, as a function of the energy in the energy range of He ionization threshold to 260 eV. Green line – ADC(1)-Stieltjes result, red line – ADC(2)-Lanczos-Stieltjes result.

width at half maximum (FWHM) pulse duration of $\tau = 413$ a.u. (10 fs) and with a peak field strength of $E_{max} = 0.075$ a.u. and $E_{max} = 0.095$ a.u respectively. This two values correspond to peak intensities of $I = 1.5 * 10^{14} W/cm^2$and $I = 3.2 * 10^{14} W/cm^2$ respectively. The intensity profile of the stronger intensity infrared (IR) pulse is shown in fig. 13. The time-dependence of the ground-state depopulation which occurs during the interaction of the Ar atom with the strong IR field is given by $1 - \rho_0(t) = 1 - \mid C_0(t) \mid^2$ and it is plotted in Fig. 13 as well.

In the Ar HHG spectrum calculation, the size of the computational box, R_{max}, is dictated by the semiclassical picture of the process [40], i.e. it must be large enough to contain the longest recolliding electronic trajectories. The classical quiver amplitude of the electron for the higher intensity pulse we are using is $r_{HHG} = \frac{E_{max}}{\omega^2} = 30 a.u.$. The calculation has been done with a radial grid radius $R_{max} = 120$ and 200 radial grid points (B-spline basis set 5, see Table I). A complex absorbing potential (CAP) has been used in order to eliminate wave-packet reflection

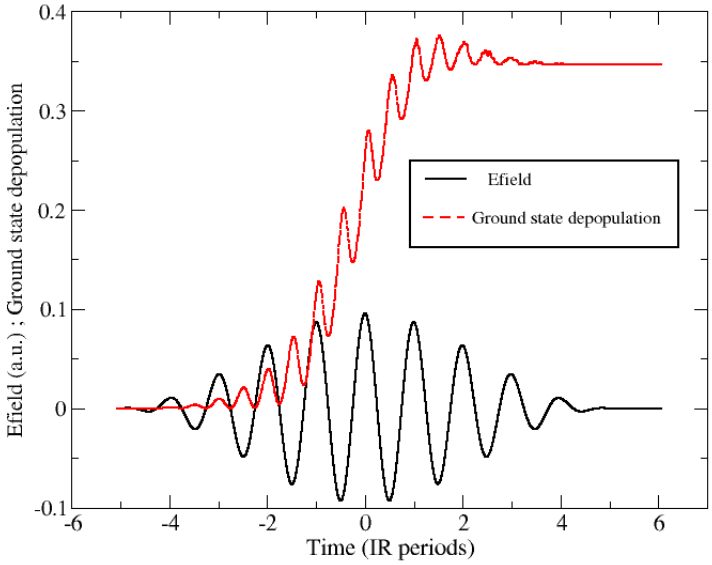

Figure 13: Time dependent IR electric field and ground state depopulation of Ar atom. The IR peak intensity is $3.2 * 10^{14} W/cm^2$.

effects from the grid boundaries. The form of the CAP used was the following:

$$\hat{W} = \eta(r - r_{CAP})^2 \tag{25}$$

and with the addiction of the CAP term the form of the total time-dependent Hamiltonian of the system reads

$$\hat{H} = \hat{H}_0 + \hat{z}E(t) - i\hat{W} \tag{26}$$

where $\hat{H}_0$ is the field-free Hamiltonian and $\hat{z}E(t)$ is the laser-atom interaction in length form and within the dipole approximation. The CAP starts at a radius $r_{CAP} = 100 a.u.$ and has a strength $\eta = 0.0005$. The maximum angular momentum employed was $l_{max} = 70$.

The HHG spectral intensity profile is shown in fig. 14, for both the two different IR intensities used. The smaller intensity used gives a cutoff energy for the HHG emission at about 50 eV. The photon energy range of 30-50 eV corresponds to a recollision electron energy range of 15-35 eV and therefore no Cooper minimum is observed in the corresponding HHG spectrum. On

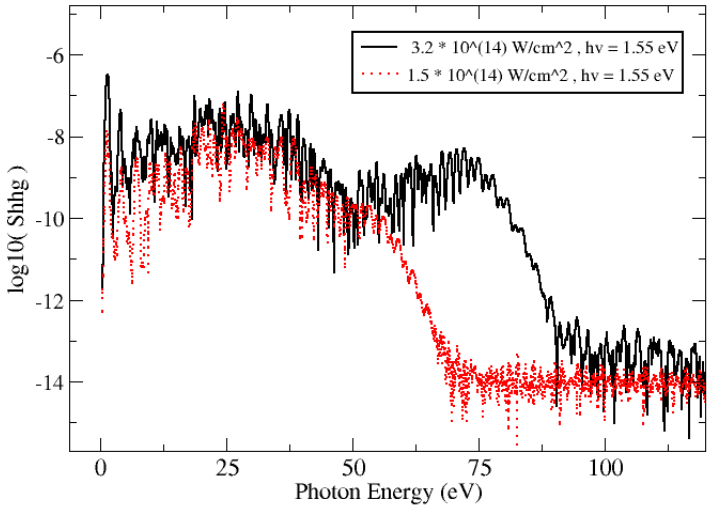

Figure 14: ADC(1) high harmonics generation emission spectrum of Ar atom interacting with an IR field. The red and black curves refer to the $1.5 * 10^{14} W/cm^2$ and $3.2 * 10^{14} W/cm^2$ values for the IR peak intensity respectively. The time duration of the IR laser pulse used is about 21 fs and the frequency is 800 nm.

the contrary, the higher intensity allows higher kinetic energies for the returning electrons, and therefore makes it possible to see the Cooper minimum shape in the HHG spectrum.

Our simulation shows that the Cooper minimum in the HHG spectra can be reproduced by the B-spline TDADC method and its position indeed lies slightly above 50 eV as found in the recent experiments [37]. The results are also in good agreement with those of Ref. [41], obtained using the time-dependent CIS technique. The position of the HHG Cooper minimum is very much consistent with the photoionization cross-section one. This has to do with the final step of the HHG process [40], where the laser-driven continuum electron recombines into the ground state emitting a single photon in a process that is directly reversed relative to the photoionization.

VII. CONCLUSIONS

In the present paper, we have presented the B-spline implementation of the first- and second-order ADC schemes for electronic excitations. By performing a series of atomic photoionization cross-section calculations, we have demonstrated the advantages of the B-spline ADC and by calculating the HHG spectrum of Ar atom we have presented the first strong-field time-dependent application of the new *ab initio* technique. In particular, we have been able to correctly predict the argon Cooper minimum shape and position both in the total cross-section, within the moment theory technique, and in the HHG spectrum. The superior accuracy of the newly implemented basis set is manifested also by the ability to correctly reproduce the high-energy tails of the cross-sections that we have shown to present a notorious difficulty for the GTO-based schemes [16]. They are indeed reproduced by the B-spline ADC in excellent agreement with the experiment.

Apart from the strongly improved accuracy, the B-spline implementation leads to a remarkable stability of the cross-sections with respect to the order of the Stieltjes-Chebyshev moment theory. While the moment theory method leads to the straightforward comparison between the performance of the GTO and B-spline bases, it is no longer a necessity within the B-spline ADC. Indeed, one can obtain directly the correctly normalized continuum eigenstates at arbitrary values of the energy in the electronic continuum by employing methods of Refs. [27, 42]. This should be one of the directions for future work. Another plausible direction of future work is generalization of the B-spline implementation to calculation of the decay widths within the Fano-Feshbach formalism, see Refs. [43] on the GTO-based Fano-ADC methods.

In view of the large (compared to GTO) size of the B-spline bases, optimized implementation of the B-spline method within the MPI and OpenMP protocols has been realized, making the future calculations of molecular systems entirely possible. The CPU time required for the cross-section calculations presented in this paper is of the order of a few minutes for the ADC(1) method and of a few hours for the ADC(2) level of theory, when using 20 computational cores.

While photoionization cross-sections are natural computational targets for the newly implemented technique, our main goal for future works is the application of the time-dependent many-

electron theory for atomic and molecular interaction with strong IR and attosecond XUV laser pulses with applications to strong field multiphoton ionization, creation of ionic state wavepackets by "sudden" single-photon ionization, high-order harmonic generation, above-threshold ionization, electron correlation-driven hole migration, etc. The present development paves the way to *ab initio* study of these phenomena beyond single excitation theory (e.g. TDCIS [41, 44]), as is indeed essential, e.g. in order to describe the dynamical phenomena involving photoabsorption from excited states of the system [17].

Acknowledgments

The authors acknowledge the EU support through the Marie Curie ITN CORINF. V.A. acknowledges the financial support of the Engineering and Physical Sciences Research Council (EPSRC, UK) through the Career Acceleration Fellowship (award EP/H003657/1) and the Programme Grant on Attosecond Dynamics (award EP/I032517).

---

[1] L. S. Cederbaum, in *The Encyclopaedia of Computational Chemistry*, edited by P. v. R. Schleyer, N. L. Allinger, T. Clask, J. Gasteiger, P. A. Kollmann, H. F. Schaefer III, and P. R. Schreiner (Wiley, Chichester, 1998).

[2] J. Schirmer, Phys. Rev. A **26**, 2395 (1982).

[3] J. Schirmer and A. Barth, Z. Phys. A **317**, 267 (1984); A. Tarantelli and L.S. Cederbaum, Phys. Rev. A **39**, 1656 (1989).

[4] A. Tarantelli and L. S. Cederbaum, Phys. Rev. A **46**, 81 (1992).

[5] F. Mertins, J. Schirmer and A. Tarantelli, Phys. Rev. A **53**, 2153 (1996); F. Mertins and J. Schirmer, Phys. Rev. A **53**, 2140 (1996); J. Schirmer and F. Mertins, J. Phys. B **29**, 3559 (1996).

[6] J. Schirmer, Phys. Rev. A **43**, 4647 (1991).

[7] J. Schirmer and A. B. Trofimov, J. Chem. Phys. **120**, 11449 (2004).

[8] A. B. Trofimov and J. Schirmer, J. Chem. Phys. **123**, 144115 (2005).

[9] Y. Velkov, T. Miteva, N. Sisourat and J. Schirmer J. Chem. Phys. **135**, 154113 (2011).

[10] B. N. Parlett, *The Symmetric Eigenvalue Problem* (Prentice-Hall, NJ, 1980).

[11] H.-D. Meyer and S. Pal, J. Chem. Phys. **91**, 6195 (1989).

[12] H.-G. Weikert, H.-D. Meyer, L. S. Cederbaum and F. Tarantelli, J. Chem. Phys. **104**, 7122 (1996).

[13] P. Langhoff, Chem. Phys. Lett. **22**, 60 (1973); P. W. Langhoff, C. T. Corcoran, J. S. Sims, F. Weinhold, and R. M. Glover, Phys. Rev. A **14**, 1042 (1976); P. Langhoff, in *Electron-Molecule and Photon-Molecule Collisions*, edited by T. Rescigno, V. McKoy, and B. Schneider (Plenum, New York, 1979) p. 183; P. W. Langhoff, in *Theory and Application of Moment Methods in Many-Fermion Systems*, edited by B. J. Dalton, S. M. Grimes, J. P. Vary, and S. A. Williams (Plenum, New York, 1980) p. 191; R. R. Whitehead, in *Theory and Applications of Moment Methods in Many-Fermion Systems*, edited by B. J. Dalton, S. M. Grimes, and J. P. Vary (Plenum, New York, 1980) p. 235; P. W. Langhoff and C. T. Corcoran, J. Chem. Phys. **61**, 146 (1974).

[14] S. Kopelke, K. Gokhberg, L. S. Cederbaum, F. Tarantelli and V. Averbukh, J. Chem. Phys. **134**, 024106 (2011); S. Kopelke, K. Gokhberg, V. Averbukh, F. Tarantelli, and L. S. Cederbaum, J. Chem. Phys. **134**, 094107 (2011).

[15] K. Gokhberg, V. Vysotskiy, L. S. Cederbaum, L. Storchi, F. Tarantelli, and V. Averbukh, J. Chem. Phys. **130**, 064104 (2009).

[16] M. Ruberti, R, Yun, K. Gokhberg, S. Kopelke, L. S. Cederbaum, F. Tarantelli, and V. Averbukh, J. Chem. Phys. **139**, 144107 (2013).

[17] M. Ruberti, R, Yun, K. Gokhberg, S. Kopelke, L. S. Cederbaum, F. Tarantelli, and V. Averbukh, J. Chem. Phys. **140**, 184107 (2014).

[18] J.W. Cukras, P. Decleva, and S. Coriani, J. Chem. Phys. **139**, 094103 (2013).

[19] I. Cacelli, V. Carravetta, A. Rizzo, and R. Moccia, Phys. Rep. **205**, 283 (1991).

[20] H. Bachau, E. Cormier, P. Decleva, J. E. Hansen and F. Martin, Rep. Prog. Phys. **64**, 1815 (2001).

[21] C. Bottcher, Phys. Rev. Lett. **48**, 85 (1982).

[22] C. Froese Fischer and M. Idrees, Comput. Phys. **3**, 53 (1989); C. Froese Fischer and W. Guo, J. Comput. Phys. **90**, 486 (1990); C. Froese Fischer, W. Guo and Z. Shen, Int. J. Quantum Chem. **42**, 849 (1992); C. Froese Fischer and M. Idrees, J. Phys. B: At. Mol. Opt. Phys. **23**, 679 (1990); T. Brage, C. Froese Fischer and G. Miecznik, J. Phys. B: At. Mol. Opt. Phys. **25**, 5289 (1992); M. Brosolo and P. Decleva, Chem. Phys. **159**, 185 (1992); M. Brosolo, P. Decleva and A. Lisini, J. Phys. B: At. Mol. Opt. Phys. **25**, 3345 (1992); T. N. Chang and T. K. Fang, Phys. Rev. A **52**, 2638 (1995); D. P. Carrol, H. J. Silverstone and R. M. Metzger, J. Chem. Phys. **71**, 4142 (1979); W. R. Johnson, S. A. Blundell and J. Sapirstein, Phys. Rev. A **37**, 307 (1988); T. N. Chang, Phys. Rev. A **39**, 4946 (1989); T. N. Chang, Phys. Rev. A **47**, 705 (1993); T. N. Chang, Phys. Rev. A **47**, 3441 (1993); T. N. Chang and X. Tang, Phys. Rev. A **44**, 232 (1991); T. N. Chang and M. Zhen, Phys. Rev. A **47**, 4849 (1993); J. C. Morrison, C. Bottcher and G. Bottrell, Theor. Chim. Acta **80**, 245

(1991); J. C. Morrison and C. Bottcher, J. Phys. B: At. Mol. Opt. Phys. **26**, 3999 (1993); Y.-T. Shen, M. Landtman and J. E. Hansen, J. Phys. B: At. Mol. Opt. Phys. **23**, L121 (1990); W. H. van der Hart and J. E. Hansen, J. Phys. B: At. Mol. Opt. Phys. **25**, 41 (1992); W. H. van der Hart and J. E. Hansen, J. Phys. B: At. Mol. Opt. Phys. **26**, 641 (1993); M. Landtman and J. E. Hansen, J. Phys. B: At. Mol. Opt. Phys. **26**, 3189 (1993); M.-K. Chen and C.-S. Hsue, J. Phys. B: At. Mol. Opt. Phys. **25**, 4059 (1992); P. Decleva, A. Lisini and M. Venuti, Int. J. Quantum Chem. **56**, 27 (1995).

[23] Raffaele Montuoro and Roberto Moccia, Chemical Physics **293** (2003) 281-308.

[24] E. Dalgaard, Int. J. Quantum Chem. **15**, 169 (1979).

[25] B. W. Shore, J. Chem. Phys. **58**, 3855 (1973).

[26] P. Lambropoulos, P. Maragakis and J. Zhang, Phys. Reports **305**, 203 (1998); E. Cormier and P. Lambropoulos, J. Phys. B: At. Mol. Opt. Phys. **30**, 77 (1997); X. Tang, H. Rudolph and P. Lambropoulos, Phys. Rev. Lett. **65**, 3269 (1990); E. Cormier and P. Lambropoulos, J. Phys. B: At. Mol. Opt. Phys. **28**, 1667 (1996); E. Cormier and P. Lambropoulos, J. Phys. B: At. Mol. Opt. Phys. **30**, 3095 (1997); R. Hasbani, E. Cormier and H. Bachau, J. Opt. Soc. Am. B **16**, 1880 (1999); P. Lambropoulos, P. Maragakis and E. Cormier, Laser Phys. **8**, 625 (1998); L. A. A. Nikolopoulos and P. Lambropoulos, Phys. Rev. Lett. **82**, 3771 (1999); S. J. Van Enk, J. Zhang and P. Lambropoulos, J. Phys. B: At. Mol. Opt. Phys. **30**, L17 (1997); J. Zhang and P. Lambropoulos, Phys. Rev. Lett. **77**, 2186 (1996); E. Cormier and M. Lewenstein, Eur. Phys. J. D **12**, 227 (2000); U. Andiel, G. D. Tsakiris, E. Cormier and K. Witte, Eur. Lett. **47**, 42 (1999); P. Maragakis, E. Cormier and P. Lambropoulos, Phys. Rev. A **60**, 4718 (1999); G. Duchateau, C. Illescas, B. Pons, E. Cormier and R. Gayet, J. Phys. B: At. Mol. Opt. Phys. **33**, L571 (2000); R. Hasbani, E. Cormier and H. Bachau, J. Phys. B: At. Mol. Opt. Phys. **33**, 2101 (2000); G. Lagmago Kamta, T. Grosges, B. Piraux, R. Hasbani, E. Cormier and H. Bachau, J. Phys. B: At. Mol. Opt. Phys. **34**, 857 (2001); E. Cormier, D. Garzella, P. Breger, P. Agostini, G. Chriaux and C. Leblanc, J. Phys. B: At. Mol. Opt. Phys. **34**, L9 (2001).

[27] P. Decleva, A. Lisini and M. Venuti, J. Phys. B: At. Mol. Opt. Phys. **27**, 4867 (1994).

[28] B. Chapman, G. Jost and R. van der Pas, *Using OpenMP: Portable Shared Memory Parallel Programming* (The MIT Press Cambridge, Massachusetts, 2007).

[29] M. Snir, S. Otto, S. Huss-Lederman, D. Walker, and J. Dongarra, *MPI: The Complete Reference* (The MIT Press Cambridge, Massachusetts, 1996).

[30] A. Szabo and N. S. Ostlund, *Modern Quantum Chemistry: Introduction to Advanced Electronic Structure Theory* (Dover, New York, 1996).

[31] J.M. Bizau and F.J. Wuilleumier, J. Elec. Spec. Rel. Phen. **71**, 205 (1995).

[32] J. A. R. Samson and W. C. Stolte, J. Electron Spectrosc. Relat. Phenom. **123**, 265 (2002).

[33] Chan W. F., Cooper G., Guo X., Burton G. R. and Brion C. E., Phys. Rev. A **46**, 149 (1992).

[34] Starace A. F. 1982 Theory of atomic photoionization Handbuch der Physik, Vol. 31 ed S Flügge (Berlin:Springer).

[35] M. Stener, P. Decleva and A. Lisini, J. Phys. B: At. Mol. Opt. Phys. **28**, 4973 (1995).

[36] K. Kaufmann, W. Baumeister, and M. Jungen, J. Phys. B **22**, 2223 (1989).

[37] J. Higuet, H. Ruf, N. Thiré, R. Cireasa, E. Constant, E. Cormier, D. Descamps, E. MÃ©vel, S. Petit, B. Pons, Y. Mairesse, and B. Fabre, Phys. Rev. A **83**, 053401 (2011); A. D. Shiner, B. E. Schmidt, C. Trallero-Herrero, P. B. Corkum, J.-C. Kieffer, F. Legare and D. M. Villeneuve, J. Phys. B: At. Mol. Opt. Phys. **45**, 074010 (2012). H. J. Worner, H. Niikura, J. B. Bertrand, P. B. Corkum, and D. M. Villeneuve, Phys. Rev. Lett. **102**, 103901 (2009). J. P. Farrell, L. S. Spector, B. K. McFarland, P. H. Bucksbaum, M. Guhr, M. B. Gaarde, and K. J. Schafer, Phys. Rev. A **83**, 023420 (2011).

[38] M. Ruberti, V. Averbukh and P. Decleva, to be submitted.

[39] A. Gordon and F. Kärtner, Opt. Express **13**, 2941 (2005).

[40] P. B. Corkum, Phys. Rev. Lett. **71**, 1994 (1993).

[41] S. Pabst, L. Greenman, D. A. Mazziotti and R. Santra, Phys. Rev. A **85**, 023411 (2012).

[42] F. Martin, Phys. Rev. A **48**, 331 (1993); M. Cortes and F. Martin, J. Phys. B: At. Mol. Opt. Phys. **27**, 5741 (1994); M. Venuti, P. Decleva and A. Lisini, J. Phys. B: At. Mol. Opt. Phys. **29**, 5315 (1996); M. Venuti and P. Decleva, J. Phys. B: At. Mol. Opt. Phys. **30**, 4839 (1997); L. Argenti and R. Moccia, J. Phys. B: At. Mol. Opt. Phys. **39**, 2773 (2006).

[43] V. Averbukh and L. S. Cederbaum, J. Chem. Phys. **123**, 204107 (2005); K. Gokhberg, V. Averbukh, and L. S. Cederbaum, J. Chem. Phys. **126**, 154107 (2007); P. Kolorenč, V. Averbukh, K. Gokhberg, and L. S. Cederbaum, J. Chem. Phys. **129**, 244102 (2008).

[44] N. Rohringer, A. Gordon and R. Santra, Phys. Rev. A **74**, 043420 (2006); L. Greenman, P.J. Ho, S. Pabst, E. Kamarchik, D. A. Mazziotti and R. Santra, Phys. Rev. A **82**, 023406 (2010).